Physical-based model for the optical simulation of III-V photodiodes

G. Mugny*, D. Rideau*, J. Grebot*, J. Tillement*, I. Nicholson*, W. Letka*, P. Fonteneau*
* STMicroelectronics, Technology and Design Platforms and Imaging Division, France

***Abstract*—In this paper, a physical-based model is presented for the optical properties of III-As ternary alloys. The model is based on the accurate description of the critical energy positions, which are computed within the Virtual Crystal Approximation (VCA) in a Tight-Binding (TB) framework, accounting for strain. Optical transitions near the band edge are described by an analytic expression, derived from Fermi Golden Rule theory, where matrix elements are supposed constant with wavevector; while higher energy transitions are described by a Dielectric Function Parametric Model (DFPM). We apply this model to InGaAs photodiode, which is simulated with Finite Difference Time Domain (FDTD) electromagnetic solver.**

I. Introduction

III-V alloys have been studied and characterized for decades and are widely used in the semiconductor industry, to manufacture optoelectronic devices, such as photodiodes, Single-Photon Avalanche Diode (SPADs) and lasers [1]. Among these alloys, $In_xGa_{1-x}As$ (hereafter InGaAs) alloys is of great interest, due to its high mobility, high photoluminescence and good epitaxial quality - in particular $In_{0.53}Ga_{0.47}As$ which is lattice-matched to InP. However, alternative substrates and alloys can also be considered [2] and potential remaining strain can affect the photodiode performances. An analytic model able to predict the optical properties of strained InGaAs alloys for composition $x \neq 0.53$ is thus of great interest.

While analytic models for the InGaAs absorption cœfficient have been proposed in the 70s and 80s (e.g. [3], [4]), they are only valid for unstrained materials and only few experimental data were available at the time. Recently, new experimental data have been published [5], [6] and its band structure has been described in details with *ab initio* methods [7]. While *ab initio* calculations show accurate results for the prediction on random alloy band structure, as well as dielectric constant, they remain numerically costly and not practical to study a vast domain of strain and composition, as required for the purpose of device simulation.

A semi-empirical and versatile model is described here, valid in the visible, NIR and SWIR region for direct band gap transitions and embedded in a commercial FDTD tools [8], to predict InGaAs photodiodes performances.

II. Methodology

A. Critical energy points: TB study

In this paper, and following [9], [10], critical transition energies for InGaAs are computed with a $sp^3d^5s^*$ TB VCA model, using parameters from [11], [12]. The band structure of unstrained $In_{0.53}Ga_{0.47}As$ is shown in Fig. 1 as reference. Critical transitions energies are also shown with red arrows.

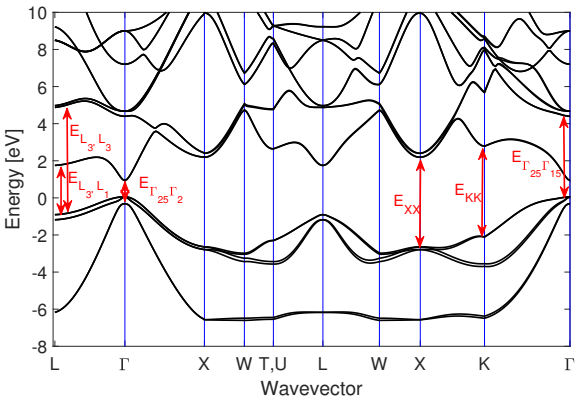

Fig. 1. Band structure of unstrained $In_{0.53}Ga_{0.47}As$ obtained by TB model. The red arrows show the main optical transitions, which are also reported in the Fig. 6.

Note that the position of E_X et E_L satellite valleys compares favourably with experimental data [13], as well as recent *ab initio* calculations, as shown in Fig. 2.

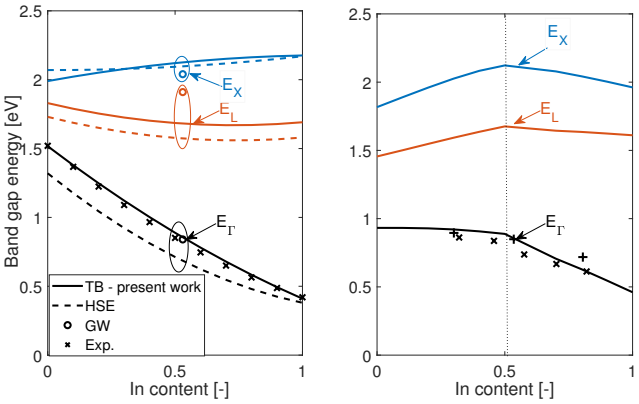

Fig. 2. Main band gap energies of unstrained (left) and biaxially strained (right) InGaAs alloys as a function of In content. Solid lines are our own TB calculation. Dashed lines are HSE calculations from [7]. Round circle are GW calculations from [14]. Experimental data, shown with cross symbols, are from [12]. Biaxial strain is computed for the case of (100) InGaAs thin layer on InP wafer. The vertical dotted line in the right figure indicates unstrained $In_{0.53}Ga_{0.47}As$ /InP.

TB models also allows to describe strained alloys, with position-dependant parameters taken from [15]. In order to

account for epitaxial strain (typically InGaAs grown on InP buffer), the *in-plane* lattice parameter is fixed to the buffer one and only the atomic position inside the cell are relaxed, as well as the outplane lattice parameter. Note that only (100) biaxial strain is considered in this study, but the calculation method can be extended to any strain orientation.

The band gap of strained InGaAs/InP obtained with this method is in good agreement with experimental gap, as shown in Fig. 2.

B. Critical energy points: compact model

To be used in a compact model, the fundamental gaps and critical transition energies can be fitted by the following law:

$$E^0_{In_xGa_{1-x}As} = E^0_{GaAs}(1-x) + E^0_{InAs}x + b_w x(1-x) \quad (1)$$

where b_w is the so-called bowing cœfficient. The parameters extracted from TB are listed in Table 8 for unstrained alloy at $T = 0$K.

In the case of biaxial strain layers, the fundamental gaps and critical transitions are fitted with the expression:

$$E_g(\epsilon) = \begin{cases} E^0_g - a_n \cdot \epsilon, & \text{if } \epsilon < 0. \\ E^0_g - a_p \cdot \epsilon, & \text{otherwise.} \end{cases} \quad (2)$$

where a_n and a_p are fitting parameter for, resp., the negative (compressive) and positive (tensile) strain (see Fig. 3). ϵ hereafter corresponds to the parallel (or *in-plane*) strain value along [100] and [010] ($\epsilon = \epsilon_{xx} = \epsilon_{yy}$).

It ought to be mentioned that the band gap variations can also be derived from the deformation potential theory directly [16], which considers linear shift of the band edge with strain and may account for hydrostatic and shear strain. However, while the deformation potential of fundamental gaps can be found in the literature, the variation of higher energy transitions are usually unknown, and the linear approximation may fail for high strain values.

Finally, the temperature dependence is described by the formula:

$$E_g(T) = E^0_g - 5.8\cdot10^{-4}\frac{T^2}{T+300}x - 4.19\cdot10^{-4}\frac{T^2}{T+271}(1-x) \quad (3)$$

where T is expressed in K and E^0_g is band gap at $T = 0$K.

C. Optical absorption at the band edge

In the absence of phonon, the optical absorption can be derived from the first-order perturbation theory by the following expression [4], [18]:

$$\alpha_{direct}(\omega) = \frac{4\pi^2e^2}{ncm^2\omega}\sum_{v,c}\int_{BZ}\frac{2}{(2\pi)^3}dk\,|e\cdot M_{cv}(k)|^2 \quad (4)$$
$$\delta(E_c(k) - E_v(k) - \hbar\omega)$$

where:

$$e\cdot M_{cv}(k) = \langle\psi_{ck}|e\cdot p|\psi_{vk}\rangle$$

This equation can be solved numerically, within semi-empirical models such as TB or Empirical Pseudopotential Method (EPM) [19], or within *ab initio* methods, such as DFT or GW [20]. However, while the electronic state are well described, the oscillator strength associated with each transition can be strongly affected by exciton effects, and one must go beyond independent particle models to accurately describe them (e.g. Time-Dependant DFT and Bethe-Salpeter equation).

Assuming parabolic dispersion near the transition and constant matrix elements, the absorption cœfficient in Eq. 4 can be simplified as [4]:

$$\alpha(\hbar\omega) = A\frac{(E_g - \hbar\omega)^{1/2}}{\hbar\omega} \quad (5)$$

where A is a fitting parameter (see Table 5), $\hbar\omega$ is the photon energy and E_g is the transition energy, computed by TB model.

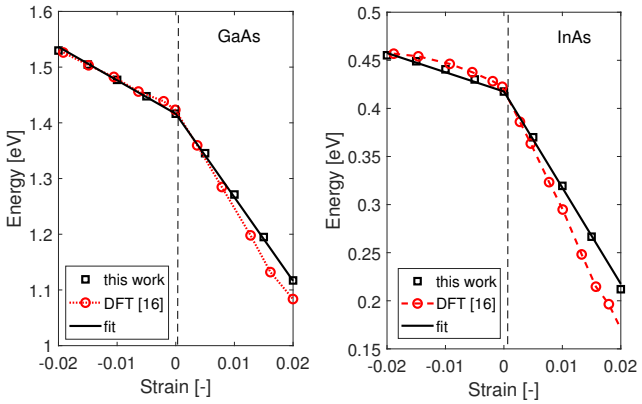

Fig. 3. Fundamental gaps at Γ for GaAs (left) and InAs (right) obtained by TB model and compared with DFT calculation from [17] in the case of biaxial strain ϵ. The fit with Eq. (2) is also shown: $a_n = 6$ and $a_p = 15$ (left) and $a_n = 2$ and $a_p = 10$ (right). The vertical dashed line is a guide to the eye for the unstrained case. ϵ corresponds to the parallel (or *in-plane*) strain value in a (100) layer.

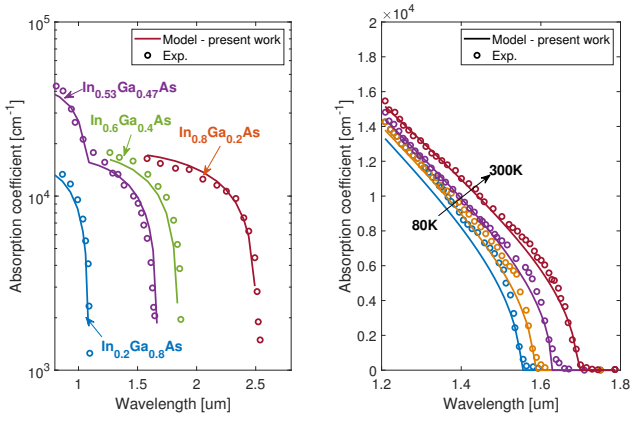

Fig. 4. Absorption cœfficient versus wavelength (left) at 300K for In content of 20, 53, 60 and 80% and (right) at temperatures between 80 and 300K for $In_{0.53}Ga_{0.47}As$. Symbols are measurement from [6] and [5], while solid lines are from Eq. (5), with transition energies from Eqs. (1) and (3) for, resp., left and right figures.

Parameters	GaAs	InAs
A_Γ (1e4 cm^{-1}eV$^{1/2}$)	3.3	2.4

Fig. 5. Parameter A reproducing experimental absorption cœfficient in Fig. 4 with Eq. 5. Parameter for InGaAs in obtained by linear interpolation.

D. Optical absorption at higher energy

For higher energy transitions, we follow the procedure from [21] and use a more pragmatic approach, combining the flexible Dielectric Function Parametric Model (DFPM) of [22] with the critical energies extracted from TB.

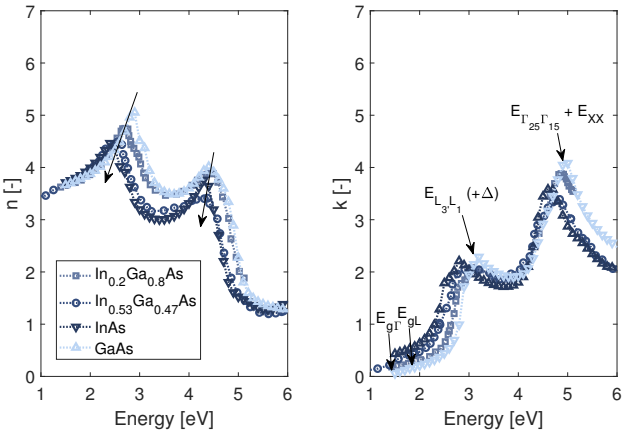

Fig. 6. Measured refractive index n (left) and extinction cœfficient k (right) for different InGaAs alloy compositions, taken from [23], [24], [25]. The critical energy transitions for GaAs are shown by arrows in the right figure, while the arrows in the left figure are guide to the eye for In content increasing.

The dielectric function is modelled as a sum of m energy-bounded polynomials that represent critical point contribution plus P Sellmeier like poles. The general expression is:

$$\begin{aligned}\varepsilon(\omega) &= \varepsilon(\omega) + i\varepsilon(\omega) \\ &= 1 + i\sum_{j=1}^{m}\int_{E_min}^{E_max} W_j(E)\phi(\hbar\omega, E, \sigma_j)\mathrm{d}E \\ &+ \sum_{j=m+1}^{m+P+1}\frac{A_j}{(\hbar\omega)^2 + E_j^2}\end{aligned} \tag{6}$$

where

$$\begin{aligned}\phi(\hbar\omega, E, \sigma_j) =& \int_0^\infty e^{i(\hbar\omega - E + i2\sigma^2 s)s}\mathrm{d}s - \int_0^\infty e^{i(\hbar\omega + E + i2\sigma^2 s)s}\mathrm{d}s \\ =& \sqrt{\tfrac{\pi}{8\sigma^2}}[e^{-y_1^2} + e^{-y_1^2}\mathrm{erf}(iy_1) - e^{-y_2^2} - e^{-y_1^2}\mathrm{erf}(iy_2)],\end{aligned} \tag{7}$$

$$y_1 = \frac{\hbar\omega - E}{2\sqrt{2}\sigma} \text{ and } y_2 = \frac{\hbar\omega + E}{2\sqrt{2}\sigma}, \tag{8}$$

$$W_j(E) = \sum_{k=0}^{N} P_{j,k}E^k u(E - a_j)u(E - b_j), \tag{9}$$

where u is the unit step function. Details on functions and parameter definitions can be found in [22].

The peak energy positions are fixed by critical energy transitions extracted from TB (as shown in Fig. 6), while other parameters are fitted in order to reproduce the experimental data available.

III. Results and Discussion

A. Optical absorption

For near band edge transitions, a good agreement between Eq. (5) and experimental data is shown in Fig. 4 for unstrained InGaAs in the NIR/SWIR wavelengths, with parameters in Table 5. For $In_{0.53}Ga_{0.47}As$, the bump around 1μm in the absorption cœfficient comes from L satellite valley contribution, showing the importance to include higher energy transitions in the model. The same parameter is considered here for E_Γ and E_L transitions ($A_L = A_\Gamma$ from Table 5).

For optical properties in the visible wavelengths, the critical transitions extracted from TB (see Table 8) are used to define the position of oscillators of the DFPM model. After carefully fitting the other parameters, a good agreement with experimental data is shown in Fig. 7 for GaAs. As the DFPM model has the advantage of accepting linear interpolation of its parameters, it is well suited to model alloy dielectric functions [21], [26] and extend it to InGaAs with different composition (not shown). All parameters used to generate Fig. 7 and model InGaAs spectrum are available upon request to the authors.

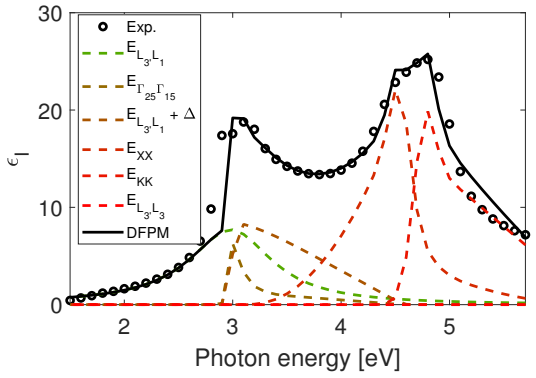

Fig. 7. Imaginary part of the dielectric function of GaAs. Symbols are measurement data from [24], while solid lines is obtained with DFPM model. The color dashed lines are showing the eight energy-bounded polynomials ($m = 8$) used for the fit, with energy values extracted from TB and shown in Table 8.

The predicted absorption cœfficient for biaxially strained InGaAs is shown in Fig. 9, for In content near 53% and strain between -2% and $+2\%$. As expected from the band edge positions, the absorption in the SWIR wavelength can be strongly enhanced with a small tensile strain, while compressive strain has less effect, or slightly reduced it. It ought to be noted that, in this case, only near-band edge absorption has been considered, using Eq. (5), but the same methods can be applied to visible and DFPM model.

Parameters	GaAs	InAs	b_w
E_Γ (eV)	1.52	0.41	-0.30
E_L (eV)	1.83	1.69	-0.30
E_X (eV)	1.99	2.18	+0.15
$E_{\Gamma_{25}\Gamma_{15}}$ (eV)	4.50	4.25	-0.11
$E_{L_{3'}L_1}$ (eV)	2.92	2.52	-0.21
$E_{L_{3'}L_3}$ (eV)	6.15	5.56	-0.20
E_{XX} (eV)	4.93	4.72	+0.08
E_{KK} (eV)	5.14	4.69	-0.16

Fig. 8. Band gaps and bowing cœfficients reproducing TB results in Fig.2 with Eq. (1) for unstrained InGaAs (top) and reproducing critical energy points highlighted in Fig.1 (bottom).

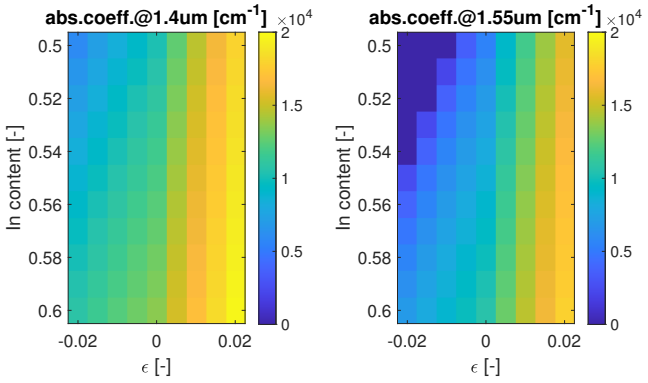

Fig. 9. Absorption cœfficient versus In content and biaxial strain at 1.4μm (left) and 1.55μm (right) wavelength and $T = 300$K. ϵ corresponds to the parallel (or *in-plane*) strain value in (100) InGaAs thin layer.

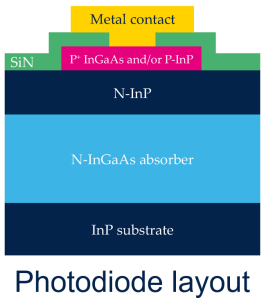

Fig. 10. InGaAs photodiode structure (reproduced from [1]). InGaAs absorber thickness in 1μm.

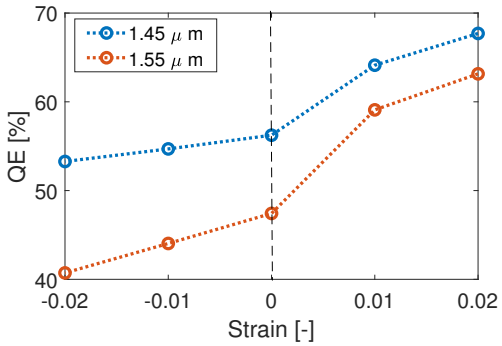

Fig. 11. QE as a function of biaxial strain at 1.45μm and 1.55μm wavelength at 300K for the InGaAs/InP PD structure of Fig. 10. Biaxial strain values are theoretically achievable, but finding the relevant process is beyond the scope of this study.

B. Photodiode simulation

Finally, the InGaAs photodiode structure in Fig. 10 is simulated by FDTD simulation [8], using the modelled InGaAs absorption cœfficient. The light comes from InP substrate and the absorber thickness is 1μm. InGaAs absorber is considered strained on InP, thus In content and biaxial strain vary together[1]. The simulated Quantum Efficiency (QE) is shown in Fig. 11. As expected, it increases with tensile strain at both 1.45 and 1.55μm wavelength, and can span from 40% to nearly 65% at 1.55μm.

IV. Conclusion

Following previous study and methodology applied to SiGeC [9], [21], the absorption cœfficient of strained and unstrained InGaAs alloys is studied. The description of the critical point transitions through TB model allows to predict the absorption cœfficient at any temperature, strain and In content, which help the development of novel InGaAs photodiode designs. The model accounts for near band edge and high energy absorption, through a DFPM model. A fully compact expression suitable for FDTD solver has been derived and used to model an InGaAs photodiode. The presented model can be extended to any III-V alloys with direct band gaps, including quaternary InGaAsP, aiming at improving strain engineering in III-V optoelectronic devices.

[1]Note that the strain values used are hypothetical and $\pm 2\%$ strain cannot physically be achieved in an homogeneous 1μm absorber thickness, which is well above the critical thickness. However, heterostructure or superlattices, which integrate thin layers with different composition/materials, could allow to relieve constraint and explore extra compositions and strain [2].

References

[1] J. Tillement, *et al.*, *Sensors*, 2023.
[2] V. Letka *et al.*, *ACS photonics*, 2023.
[3] S. Adachi, *Journal of Applied Physics*, 1989.
[4] F. Bassani *et al.*, *Electronic States and Optical Transitions*, 1975.
[5] M. Verdun, Ph.D. dissertation, Université Paris Saclay, 2016.
[6] H. J. Lee *et al.*, *Journal of Electronic Materials*, 2022.
[7] P. A. Khomyakov *et al.*, *Applied Physics Letters*, 2015.
[8] Lumerical, *Inc., 2024-r2 edition*, 2024.
[9] D. Ridean *et al.*, in *Proc. SISPAD*, 2023.
[10] D. Rideau *et al.*, *Physical Review B*, 2006.
[11] J. Jancu *et al.*, *Physical Review B*, 1998.
[12] I. Vurgaftman *et al.*, *Journal of applied physics*, 2001.
[13] G. Mugny *et al.*, in *Proc.SISPAD*, 2015.
[14] G. Greene-Diniz *et al.*, *Journal of Applied Physics*, 2016.
[15] M. Nestoklon *et al.*, *Journal of Physics: Condensed Matter*, 2016.
[16] C. G. Van de Walle, *Physical review B*, 1989.
[17] M. Rau *et al.*, in *Proc. ESSDERC (IEEE)*, 2016.
[18] C. Delerue and M. Lannoo, 2013.
[19] C. Kriso *et al.*, *Solid-State Electronics*, 2017.
[20] G. Onida *et al.*, *Reviews of modern physics*, 2002.
[21] J. Grebot *et al.*, in *Proc. ESSDERC (IEEE)*, 2021.
[22] C. M. Herzinger and B. D. Johs, 1998, uS Patent 5,796,983.
[23] D. E. Aspnes and A. Studna, *Physical review B*, 1983.
[24] D. Aspnes *et al.*, *Journal of applied physics*, 1986.
[25] IOFFE, https://www.ioffe.ru/SVA/NSM/Semicond/.
[26] C. Emminger *et al.*, *Journal of Vacuum Science & Technology B*, 2020.